Numerical Analysis of Dissipative and Magnetized Reiner-Philippoff Nanofluid with Activation Energy and Cattaneo-Christov Double Diffusion Model

M. Adel[1,*], M. M. Khader[2,3], I. Alradaddi[1], A. Alaidrous[4], N. A. Mohammed[4], G. M. Ismail[1]

[1] *Department of Mathematics, Faculty of Science, Islamic University of Madinah, Medina, Saudi Arabia*

[2] *Department of Mathematics and Statistics, College of Science, Imam Mohammad Ibn Saud Islamic University (IMSIU), Riyadh, Saudi Arabia*

[3] *Department of Mathematics, Faculty of Science, Benha University, Benha, Egypt*

[4] *Mathemtaics Department, Faculty of Sciences, Umm Al-Qura University, Makkah, Saudi Arabia*

Abstract. We perform an investigation using numerical simulations to examine the influence of magnetohydrodynamics and thermal radiation on the mass transport and thermal energy properties of non-Newtonian Reiner-Philippoff nanofluids. We thoroughly examine the species response concerning activation energy, thermal radiation at the surface, viscous dissipation, Cattaneo-Christov double diffusions, and mass and energy transfer. This analysis also examines the impacts of an applied transverse magnetic field and Ohmic heating. Using appropriate similarity variables converts the specified governing system of PDEs into a non-linear system of ODEs. We numerically solve the governing equations using the Mohand transform (MT) in conjunction with the Adomian decomposition method (ADM). The sophisticated Modified Decomposition Method (MDM) streamlines complex equations for computational solutions. It uses ADM and the MT to make sure that the series converges, giving a solution very close to the exact solution. We illustrate the temperature, species distributions, and flow velocity for the relevant parameters governing the Reiner-Philippoff model on two-dimensional charts to understand the influence of dimensionless parameters on these values. The tabulation, depiction, and interpretation of the local Nusselt number, local Sherwood number, and skin friction coefficient exemplify further engineering inquiry. We have utilized a table to illustrate the concordance between the current numerical data and previously published findings.

2020 Mathematics Subject Classifications: 41A30, 76F12, 65M60, 65N12.

Key Words and Phrases: Activation energy, Nanofluid, Cattaneo-Christov double diffusions, Reiner-Philippoff model, Mohand transforms, ADM.

---

1. Introduction

The study of non-Newtonian fluids has attracted a lot of interest because of its numerous uses in various industrial settings, such as drilling rigs, food processing, cooling systems, nuclear reactors, and organic material handling. These fluids are especially well suited for these intricate and demanding situations because of their distinctive flow behaviors. Because of this, it is now essential to comprehend their characteristics and behaviors to maximize productivity and efficiency in these sectors. Non-Newtonian liquids can be represented by several models that are frequently used in technology and engineering domains. Examples of these models include the Gingham plastic model, Sisal model, Carrell-Cauda model, Jeffrey model, Caisson model, Power-law model, Ellipse model, and Jeffrey model. We explore a particular kind of non-Newtonian model called the Reiner-Philippoff fluid [16] in this work. This model stands out in particular because of its distinct rheological characteristics, which make it useful for a wide range of real-world applications. The goal of this study is to gain a better understanding of the Reiner-Philippoff fluid and its possible use in industrial processes where conventional fluid assumptions are not applicable. Several researchers have thoroughly examined the Reiner-Philippoff model. For in-depth analyses and research on this subject, see references like ([2], [12], [13], [20]). These studies offer insightful information about the properties and uses of the Reiner-Philippoff fluid, facilitating a better comprehension of its behavior in diverse settings.

In the same area of research, there are many researchers studied the same and similar problems for example ([11], [22], [21]): The authors conducted a comparative analysis of flow and Cattaneo-Christov heat flux in the presence of a magnetic field, taking into account the influence of nonmaterial and carbon annotations. The researchers also looked at magnetic swirling flow and the Cattaneo-Christov heat and mass flux over a stretchable cylinder. They also looked at how heat moves and melts in a Reiner-Philippoff fluid on a Darby-Herxheimer medium.

One important natural occurrence is the movement of heat between two objects or within one object. Numerous academic fields rely heavily on this process: thermodynamics, where it is critical to comprehending energy systems; meteorology, where it impacts weather patterns and climate; engineering, where it is essential to the design and operation of machinery and structures; environmental science, where it impacts ecological dynamics; and material science, where it affects the characteristics and capabilities of various materials. The Cattaneo-Christov heat flux model is the name given to this intricate mathematical structure. It offers a more realistic representation of non-Fourier heat conduction phenomena by taking into account thermal relaxation effects, which is an advanced method of explaining heat transfer [9]. Accurately describing thermal conduction-especially in dynamic situations is one of the advantages of the Cattaneo-Christov heat flux model for heat transfer studies. For accurate forecasts in sectors like biotechnology and high-speed thermal processes, it is crucial to consider time-dependent effects including thermal relaxation, which is not possible with Fourier's equation. Numerous investigations ([7], [8], [19]) have been motivated by the significance and broad uses of this concept. Also, different numerical techniques studied many important problems like ([6], [10]), the authors presented

numerical methods for solving the Laplace equation's IBM; finite difference methods underpin the method. Also, the authors numerically solved the period of a simple pendulum in a magnetic field.

These days, nanofluid investigations are receiving a lot of interest due to their amazing applications in engineering, science, and technology. Chop [5] came up with the idea of nanofluids first. Because of their improved thermal and lubricating qualities, panotitides are used in machining processes such as milling and turning. By examining the consequences of suspending different nonmaterials in fluids, scientists ([1], [4], [15]) have significantly advanced our understanding of nanofluid flow. With continuous study aimed at exploring and optimizing the efficiency of these sophisticated fluids in industrial applications, this focus has grown, especially in the current decade.

The concerned model simplifies to a system of extremely nonlinear ordinary differential equations. These equations are inherently nonlinear, hence it is impossible to discover an accurate analytical solution. As such, to derive an approximation of the solution, a strong numerical technique must be used. We can manage the system's complexity and obtain practical numerical results with this method. We addressed the given problem analytically by applying a recently developed methodology. The modified decomposition method replaces the classic Adomian decomposition technique with the Mohand transform, employed in this strategy. This new approach offers greater accuracy and efficiency, which makes it a significant advance in solving difficult analytical problems. Through the application of the Mohand transform ([17], [18]), the enhanced decomposition method optimizes the solution process and yields more precise outcomes across a broader spectrum of applications. The MDM provides multiple-form solutions, culminating in the exact form solution. The solution to the resultant nonlinear system of ordinary differential equations confirms the efficacy and applicability of this method. Tables and charts are employed to compare the collected data.

Building upon the insights from prior research, this study addresses a significant gap by exploring the flow dynamics of a non-Newtonian Reiner-Philippoff nanofluid over a nonlinear stretching sheet, a scenario not extensively studied in the literature. Unlike previous works, this analysis incorporates the complex effects of activation energy and the Cattaneo-Christov double diffusion model, alongside the influences of Ohmic heating and viscous dissipation, which are often overlooked in similar studies. By employing an enhanced decomposition method refined with Mohand transforms, this work provides a robust framework for tackling the challenges posed by these nonlinearities. Numerical solutions are derived and examined for a wide range of parameter values, offering new insights into the interplay of these effects. Furthermore, the method's accuracy is validated by demonstrating strong agreement with existing solutions in specific limiting cases, thereby filling a critical gap in understanding the behavior of Reiner-Philippoff nanofluids under these unique conditions.

2. Mathematical Development

In the context of magnetohydrodynamics (MHD) and thermal radiation, this section provides a thorough summary of the mathematical framework used in the numerical analysis of Reiner-Philippoff nanofluid flow encompasses the Cattaneo-Christov double diffusion model (CADDY). The magnetic field strength, denoted by $B = B_0 x^{\frac{-1}{3}}$, is defined as the fluid flow past a nonlinearly extending sheet in the study. This formulation takes into consideration both chemical interactions and viscous dissipation. The study also includes diffusion from thermophagies, denoted by D_T, and Browning diffusion, represented by D_B. This study considers activation energy since it is important for nanofluid flow and has a significant effect on the rate of thermal and chemical processes, which in turn impacts the fluid's overall behavior and performance in many applications. Characterizing the flow is a system of PDEs: the continuity equation, the momentum equation adjusted for magnetohydrodynamic phenomena, the energy equation incorporating viscous dissipation, the CCDM, the species concentration equation with activation energy phenomenon, and the chemical reactions involved. This study considers the impact of heat radiation on the sheet with the measurement and evaluation of Ohmic heating. The schematic configuration diagram illustrates the surface velocity, represented by the equation: $u_w = ax^{\frac{1}{3}}$, where a is a positive constant. Figure 1 offers a more comprehensive depiction of the flow pattern.
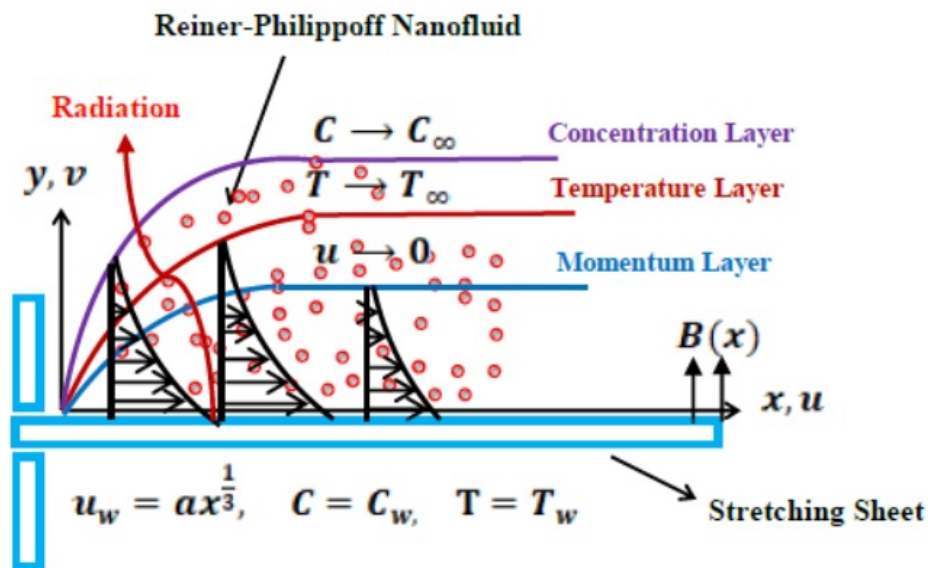

Figure 1. Modeling geometry flow

Furthermore, during the flow motion, it is posited that the pertinent temperatures remain constant. Throughout the operation, the ambient temperature T_∞, indicative of the temperature distant from the sheet, and the surface temperature T_w, denoting the temperature at the surface of the stretching sheet, are both held at constant values. For

better understanding, the assumptions made for this problem are summarized below in a list for easier comprehension.

i. Flow Geometry:

The fluid flow is modeled as two-dimensional, with a constant velocity, and exhibits laminar behavior over the stretching surface.

ii. Governing Forces:

The fluid flow is affected by the presence of a magnetic field perpendicular to the flow direction, heat transfer due to radiation, and energy dissipation caused by fluid viscosity.

iii. Diffusion Mechanism:

The species concentration dynamics are modeled using the Cattaneo-Christov double diffusion approach and incorporate activation energy effects.

iv. Similarity Transformation:

Similarity transformations are used to reduce the PDEs to a system of ODEs.

v. Numerical Methodology:

The governing equations are solved by employing the Mohand transform in conjunction with the Adomian decomposition method. The Modified Decomposition Method is utilized to guarantee the convergence of the series solution.

Considering these constraints, the governing equations for the modeled system are derived as follows [14]:

$$\frac{\partial u}{\partial x} + \frac{\partial v}{\partial y} = 0, \tag{1}$$

$$\frac{\partial u}{\partial y} = \frac{\tau}{\left(\frac{\mu_0 - \mu_\infty}{1 + \left(\frac{\tau}{\tau_s}\right)^2} + \mu_\infty\right)}, \tag{2}$$

$$u\frac{\partial u}{\partial x} + v\frac{\partial u}{\partial y} + \frac{\sigma}{\rho}B^2 u - \frac{1}{\rho}\frac{\partial \tau}{\partial y} = 0, \tag{3}$$

$$u\frac{\partial T}{\partial x} + v\frac{\partial T}{\partial y} - \frac{\kappa}{\rho c_p}\left(1 + \frac{16\sigma^* T_\infty^3}{3\kappa k^*}\right)\left(\frac{\partial^2 T}{\partial y^2}\right) - \frac{\mu}{\rho c_p}\left(\tau\frac{\partial u}{\partial y}\right) - \Omega\left[D_B\frac{\partial C}{\partial y}\frac{\partial T}{\partial y} + \frac{D_T}{T_\infty}\left(\frac{\partial T}{\partial y}\right)^2\right]$$

$$-\frac{\sigma B^2}{\rho c_p}u^2 + \Lambda_t\left[\left(u\frac{\partial u}{\partial x} + v\frac{\partial u}{\partial y}\right)\frac{\partial T}{\partial x} + \left(u\frac{\partial v}{\partial x} + v\frac{\partial v}{\partial y}\right)\frac{\partial T}{\partial y} + u^2\frac{\partial^2 T}{\partial x^2} + v^2\frac{\partial^2 T}{\partial y^2} + 2uv\frac{\partial^2 T}{\partial x\partial y}\right] = 0, \tag{4}$$

$$u\frac{\partial C}{\partial x} + v\frac{\partial C}{\partial y} + \Lambda_c\left[\left(u\frac{\partial u}{\partial x} + v\frac{\partial u}{\partial y}\right)\frac{\partial C}{\partial x} + \left(u\frac{\partial v}{\partial x} + v\frac{\partial v}{\partial y}\right)\frac{\partial C}{\partial y} + u^2\frac{\partial^2 C}{\partial x^2} + v^2\frac{\partial^2 C}{\partial y^2} + 2uv\frac{\partial^2 C}{\partial x\partial y}\right] -$$

$$D_B\frac{\partial^2 C}{\partial y^2} - \frac{D_T}{T_\infty}\frac{\partial^2 T}{\partial y^2} + K_r(C - C_\infty)\left(\frac{T}{T_\infty}\right)^n e^{\frac{-E_a}{\kappa T}} = 0. \tag{5}$$

It is important to recognize that the system under study is two-dimensional. Therefore, it is thought that there are two components to the flow velocity: u in the $x-$axis and v in the $y-$axis. τ denotes shear stress, whereas τ_s denotes the reference shear stress. Λ_t represents the relaxation time for heat flux, Ω represents the effective heat capacity ratio, and Λ_c represents the relaxation time for mass flux. ρ denotes fluid density, μ_∞ signifies ambient viscosity, ν indicates kinematic viscosity, μ_0 refers to dynamic viscosity at zero shear, and σ symbolizes electrical conductivity. The concentration of a component in the fluid is denoted by C, signifying its quantity or distribution within the fluid medium, while C_∞ denotes the ambient concentration. The thermal condition and total thermal energy of the nanofluid are indicated by its temperature, T. This value is essential because it sheds light on the thermal state of the nanofluid, affecting its behavior and thermal characteristics in a variety of applications. Particular boundary conditions apply to the regulation equations (2) through (5). By specifying the restrictions that are applied to the equations at the system's edges, these conditions also define the behavior of the system at its boundaries:

$$u = u_w(x) = ax^{\frac{1}{3}}, \qquad v = -v_w, \qquad T = T_w, \qquad C = C_w, \quad at \quad y = 0, \qquad (6)$$

$$u \to 0, \qquad C \to C_\infty, \qquad T \to T_\infty, \qquad at \qquad y \to \infty. \qquad (7)$$

2.1. Dimensionless model

We reformulated the governing equations and boundary conditions in a dimensionless format to enhance the efficacy of numerical analysis. By employing appropriate dimensionless variables, this transformation simplifies the equations, facilitating the identification of the primary variables influencing the system's behavior. This approach simplifies the analysis, highlighting critical aspects and improving our comprehension of the system's dynamics overall. Using this method simplifies the equations while highlighting the significance of the dimensionless parameters. These include the radiation parameter, the thermophoresis parameter, the chemical reaction parameter, the solutal relaxation time parameter, the Brownian motion parameter, the Eckert number, the thermal relaxation parameter, and the Prandtl number [3]:

$$\phi(\eta) = \frac{C - C_\infty}{C_w - C_\infty}, \qquad \theta(\eta) = \frac{T - T_\infty}{T_w - T_\infty}, \qquad (8)$$

$$\tau = \rho\sqrt{\nu a^3}g(\eta), \qquad \psi = \sqrt{\nu a}x^{2/3}f(\eta), \qquad \eta = y\sqrt{\frac{a}{\nu}}x^{-1/3}. \qquad (9)$$

The continuity equation is readily fulfilled by inserting (8) and (9) into equations (2)-(5). The linked nonlinear differential equations governing motion, concentration, and energy can then be derived via the subsequent techniques, yielding the following outcomes:

$$g = \left(\frac{\lambda\gamma^2 + g^2}{\gamma^2 + g^2}\right)f'', \qquad (10)$$

$$g' = \frac{1}{3}f'^2 + Mf' - \frac{2}{3}ff'', \qquad (11)$$

$$\frac{1}{\Pr}\left((R+1)\theta''\right) + M\,Ec\,f'^2 + Ec\,g\,f'' + Z_b\,\phi'\theta' + \Upsilon_t\left(\eta\,\theta''\,f^2 + f\,\theta'\,f'\right) + Z_t\,\theta'^2 + \frac{2}{3}f\theta' = 0, \tag{12}$$

$$\phi'' + \frac{Z_t}{Z_b}\theta'' - S_c\delta_r\,(1+\Gamma\,\theta)^n\,e^{\left(\frac{-E}{1+\Gamma\theta}\right)}\phi + \Upsilon_c\,S_c\left(\eta\,\phi''\,f^2 + f\,\phi'\,f'\right) + \frac{2}{3}S_c\,f\phi' = 0. \tag{13}$$

In addition, the relevant boundary conditions are modified to meet the predefined criteria listed below. This modification guarantees the fulfillment of all requirements, upholding the procedure's accuracy and uniformity. The following are the specific requirements:

$$f(\eta) = \beta, \qquad f'(\eta) = 1, \qquad \theta(\eta) = 1, \qquad \phi(\eta) = 1, \qquad at \quad \eta = 0, \tag{14}$$

$$f' \to 0, \qquad \theta \to 0, \qquad \phi \to 0, \qquad as \quad \eta \to \infty. \tag{15}$$

Now, the model under investigation has been converted to (10)-(15), the definitions of the regulating factors are as follows: The thermal relaxation parameter is represented by $\Upsilon_t = \Lambda_t u_w$, the Brownian motion parameter by $Z_b = \frac{\Omega(C_w - C_\infty)D_B}{\nu}$, the magnetic parameter can be expressed as $M = \frac{\sigma}{\rho a}B^2$, the thermophoresis parameter by $Z_t = \frac{\Omega(T_w - T_\infty)D_T}{\nu T_\infty}$, the solutal relaxation time parameter is denoted by $\Upsilon_c = \Lambda_c u_w$, the thermal radiation parameter shown by $R = \frac{16\sigma^* T_\infty^3}{3\kappa k^*}$, the dimensionless activation energy variable by $E = \frac{E_a}{\kappa T_\infty}$, the Reiner-Philippoff fluid parameter denoted by $\lambda = \frac{\mu_0}{\mu_\infty}$, the Schmidt number by $S_c = \frac{\nu}{D_B}$, the temperature relative parameter represented by $\Gamma = \frac{T_w - T_\infty}{T_\infty}$, the Prandtl number by $\Pr = \frac{\mu c_p}{\kappa}$, the Bingham number by $\gamma = \frac{\tau_s}{\rho\sqrt{a^3\nu}}$, the chemical reaction parameter by $\delta_r = \frac{K_r}{a}$ and the Eckert number by $Ec = \frac{u_w^2}{c_p(T_w - T_\infty)}$.

2.2. Important applicable quantities

Crucial and pertinent physical parameters of practical and technological importance across various domains include the local Sherwood number Sh_x, the local Nusselt number Nu_x, and the local skin friction coefficient Cf_x in the proposed physical model. The subsequent summary will help to clarify these requirements:

$$Cf_x Re^{\frac{1}{2}} = -g(0), \qquad Nu_x Re^{\frac{-1}{2}} = -(1+R)\,\theta'(0), \qquad Sh_x Re^{\frac{-1}{2}} = -\phi'(0),$$

where $Re = \frac{u_w x}{\nu}$ is the local Reynolds number.

3. Procedure Solution

3.1. Fundamental principles of the Mohand transform

Definition 1: For a function $f(t)$, the Mohand transformation indicated by $\mathbb{M}(.)$ is defined as [17]:

$$\mathbb{M}\{f(t)\} = F(s) = s^2 \int_0^\infty f(t)e^{-st}dt, \qquad k_1 \le s \le k_2.$$

If the Mohand transform of a function $f(t)$ is $F(s)$ then $f(t)$ is known as the inverse of $F(s)$ which can be described by:

$$\mathbb{M}^{-1}\{F(s)\} = f(t), \qquad \mathbb{M}^{-1} \text{ is the inverse Mohand operator.}$$

The MT of the derivatives of the function $f(t)$: If $\mathbb{M}\{f(t)\} = F(s)$ then we have

$$\mathbb{M}\left\{f^{(n)}(t)\right\} = s^n F(s) - s^{n+1}f(0) - s^n f'(0) - \ldots - s^2 f^{(n-1)}(0), \quad n = 1, 2, \ldots . \quad (16)$$

The MT for the power functions:

$$\mathbb{M}\{t^n\} = \begin{cases} \frac{n!}{s^{n-1}}, & n \in N; \\ \frac{\Gamma(n+1)}{s^{n-1}}, & n > -1. \end{cases}$$

3.2. Implementation of modified decomposition method

This part succinctly outlines the procedure of the newly adopted modified technique. To execute the MDM for addressing the proposed system (10)-(13), we will reformulate it in the subsequent operator form:

$$f''(\eta) = N^1(f,g) = \left(\frac{1}{\lambda\gamma^2}\right)\left[g\left(\gamma^2 + g^2\right) - g^2 f''\right], \tag{17}$$

$$g'(\eta) = N^2(f) = \frac{1}{3}f'^2 - \frac{2}{3}ff'' + M f', \tag{18}$$

$$\begin{aligned}\theta''(\eta) = N^3(f,g,\theta,\varphi) = \left(\frac{-Pr}{1+R}\right)&\left[M Ec\, f'^2 + Ec\, g\, f'' + Z_b\, \phi'\theta'\right.\\ &\left.+ \Upsilon_t\left(\eta\, \theta''\, f^2 + f\, \theta'\, f'\right) + Z_t\, \theta'^2 + \frac{2}{3}f\theta'\right],\end{aligned} \tag{19}$$

$$\begin{aligned}\varphi''(\eta) = N^4(f,\theta,\varphi) = &-\frac{Z_t}{Z_b}\theta'' + S_c\delta_r\,(1+\Gamma\,\theta)^n\,\phi\,Exp\left[\frac{-E}{1+\Gamma\,\theta}\right]\\ &- \Upsilon_c\,S_c\left(\eta\,\phi''\,f^2 + f\,\phi'\,f'\right) - \frac{2}{3}S_c\,f\phi'.\end{aligned} \tag{20}$$

Take the Mohand transform of this system (17)-(20) as follows:

$$\begin{aligned} s^2 F(s) - s^3 f(0) - s^2 f'(0) &= \mathbb{M}\left[N^1(f,g)\right], \\ s\, G(s) - s^2 g(0) &= \mathbb{M}\left[N^2(f)\right], \\ s^2 \Theta(s) - s^3\theta(0) - s^2\theta'(0) &= \mathbb{M}\left[N^3(f,g,\theta,\varphi)\right], \\ s^2 \Phi(s) - s^3\varphi(0) - s^2\varphi'(0) &= \mathbb{M}\left[N^4(f,\theta,\varphi)\right]. \end{aligned} \tag{21}$$

By using the boundary conditions (14)-(15), we can solve the above algebraic system as follows:

$$
\begin{aligned}
F(s) &= 1 + \frac{1}{s^2} \mathbb{M}\left[N^1(f,g)\right], \\
G(s) &= \ell_1\, s + \frac{1}{s} \mathbb{M}\left[N^2(f)\right], \\
\Theta(s) &= s + \ell_2 + \frac{1}{s^2} \mathbb{M}\left[N^3(f,g,\theta,\varphi)\right], \\
\Phi(s) &= s + \ell_3 + \frac{1}{s^2} \mathbb{M}\left[N^4(f,\theta,\varphi)\right].
\end{aligned}
\tag{22}
$$

Take the inverse Mohand transform of the system (22) as follows:

$$
\begin{aligned}
f(\eta) &= \eta + \mathbb{M}^{-1}\left[\frac{1}{s^2}\mathbb{M}\left[N^1(f,g)\right]\right], \\
g(\eta) &= \ell_1 + \mathbb{M}^{-1}\left[\frac{1}{s}\mathbb{M}\left[N^2(f)\right]\right], \\
\theta(\eta) &= 1 + \ell_2\,\eta + \mathbb{M}^{-1}\left[\frac{1}{s^2}\mathbb{M}\left[N^3(f,g,\theta,\varphi)\right]\right], \\
\varphi(\eta) &= 1 + \ell_3\,\eta + \mathbb{M}^{-1}\left[\frac{1}{s^2}\mathbb{M}\left[N^4(f,\theta,\varphi)\right]\right],
\end{aligned}
\tag{23}
$$

where

$$
\ell_1 = g(0), \qquad \ell_2 = \theta'(0), \qquad \ell_3 = \varphi'(0).
$$

Consequently, the preliminary elements for the estimated solution of the specified problem will be derived as follows:

$$
f_0(\eta) = \eta, \qquad g_0(\eta) = \ell_1, \qquad \theta_0(\eta) = 1 + \ell_2\,\eta, \qquad \varphi_0(\eta) = 1 + \ell_3\,\eta,
\tag{24}
$$

subsequently, the conclusive iterative strategy for the remaining terms is expressed as:

$$
\begin{aligned}
f_{m+1}(\eta) &= \mathbb{M}^{-1}\left[\frac{1}{s^2}\mathbb{M}\left[N^1(f,g)\right]\right] = \mathbb{M}^{-1}\left[\frac{1}{s^2}\mathbb{M}\left[A_m^1\right]\right], \\
g_{m+1}(\eta) &= \mathbb{M}^{-1}\left[\frac{1}{s}\mathbb{M}\left[N^2(f)\right]\right] = \mathbb{M}^{-1}\left[\frac{1}{s}\mathbb{M}\left[A_m^2\right]\right], \\
\theta_{m+1}(\eta) &= \mathbb{M}^{-1}\left[\frac{1}{s^2}\mathbb{M}\left[N^3(f,g,\theta,\varphi)\right]\right] = \mathbb{M}^{-1}\left[\frac{1}{s^2}\mathbb{M}\left[A_m^3\right]\right], \\
\varphi_{m+1}(\eta) &= \mathbb{M}^{-1}\left[\frac{1}{s^2}\mathbb{M}\left[N^4(f,\theta,\varphi)\right]\right] = \mathbb{M}^{-1}\left[\frac{1}{s^2}\mathbb{M}\left[A_m^4\right]\right].
\end{aligned}
\tag{25}
$$

The nonlinear terms $N^p(f,g,\theta,\varphi)$, $p = 1,2,3,4$, are decomposed by using the Adomian polynomials defined as:

$$
N^p(f,g,\theta,\varphi) = \sum_{m=0}^{\infty} A_m^q, \qquad p = 1,2,3,4,
\tag{26}
$$

where,

$$A_m^p = \frac{1}{m!} \left[\frac{d^m}{d\lambda^m} \left[N^p \left(\sum_{i=0}^{\infty} \lambda^i f_i, \sum_{i=0}^{\infty} \lambda^i g_i, \sum_{i=0}^{\infty} \lambda^i \theta_i, \sum_{i=0}^{\infty} \lambda^i \varphi_i \right) \right] \right]_{\lambda=0}, \qquad p = 1, 2, 3, 4.$$

(27)

Considering these formulas, we can calculate the initial Adomian polynomials as follows:

$$A_0^1 = \left(\frac{1}{\lambda\gamma^2} \right) \left[g_0 \left(\gamma^2 + g_0^2 \right) - g_0^2 f_0'' \right] = \left(\frac{1}{\lambda\gamma^2} \right) \left[\ell_1 \left(\gamma^2 + \ell_1^2 \right) - \ell_1^2 \ell_4 \right],$$

$$A_0^2 = \frac{1}{3} f_0'^2 - \frac{2}{3} f_0 f_0'' + M f_0' = \frac{1}{3} + M,$$

$$A_0^3 = \left(\frac{-Pr}{1+R} \right) \left[M\, Ec\, f_0'^2 + Ec\, g_0\, f_0'' + Z_b\, \phi_0'\theta_0' + \Upsilon_t \left(\eta\, \theta_0''\, f_0^2 + f_0\, \theta_0'\, f_0' \right) + Z_t\, \theta_0'^2 + \frac{2}{3}\, f_0 \theta_0' \right]$$

$$\quad = \left(\frac{-Pr}{1+R} \right) \left[M\, Ec + Ec\, \ell_1\, \ell_4 + Z_b \ell_2\, \ell_3 + Z_t \ell_2^2 \right],$$

$$A_0^4 = -\frac{Z_t}{Z_b} \theta_0'' + S_c\delta_r \left(1 + \Gamma\, \theta_0 \right)^n \phi_0\, Exp \left[\frac{-E}{1 + \Gamma\, \theta_0} \right] - \Upsilon_c\, S_c \left(\eta\, \phi_0''\, f_0^2 + f_0\, \phi_0'\, f_0' \right) - \frac{2}{3} S_c\, f_0 \phi_0'$$

$$\quad = -\frac{Z_t}{Z_b}\, \ell_5 + S_c\delta_r \left(1 + \Gamma \right)^n Exp \left[\frac{-E}{1 + \Gamma} \right].$$

(28)

Considering the iteration formulas (25), we can calculate the first components of the approximate solution as follows:

$$f_1(\eta) = \mathbb{M}^{-1} \left[\frac{1}{s^2} \mathbb{M} \left[A_0^1 \right] \right] = \left(\frac{1}{2\lambda\gamma^2} \right) \eta^2 \left[\ell_1 \left(\gamma^2 + \ell_1^2 \right) - \ell_1^2 \ell_4 \right],$$

$$g_1(\eta) = \mathbb{M}^{-1} \left[\frac{1}{s} \mathbb{M} \left[A_0^2 \right] \right] = \eta \left[\frac{1}{3} + M \right],$$

$$\theta_1(\eta) = \mathbb{M}^{-1} \left[\frac{1}{s^2} \mathbb{M} \left[A_0^3 \right] \right] = \frac{1}{2}\eta^2 \left[\left(\frac{-Pr}{1+R} \right) \left[M\, Ec + Ec\, \ell_1\, \ell_4 + Z_b \ell_2\, \ell_3 + Z_t \ell_2^2 \right] \right],$$

$$\varphi_1(\eta) = \mathbb{M}^{-1} \left[\frac{1}{s^2} \mathbb{M} \left[A_0^4 \right] \right] = \frac{1}{2}\eta^2 \left[-\frac{Z_t}{Z_b}\, \ell_5 + S_c\delta_r \left(1 + \Gamma \right)^n Exp \left[\frac{-E}{1+\Gamma} \right] \right], \ldots.$$

(29)

Consequently, the approximate solution is derived by aggregating m of the estimated terms as follows:

$$f(\eta) = \sum_{k=0}^{m-1} f_k(\eta), \qquad g(\eta) = \sum_{k=0}^{m-1} g_k(\eta), \qquad \theta(\eta) = \sum_{k=0}^{m-1} \theta_k(\eta), \qquad \varphi(\eta) = \sum_{k=0}^{m-1} \varphi_k(\eta).$$

(30)

The series form solution converges to the exact solution as m approaches infinity.

The values of the quantities ℓ_k, $k = 1, 2, 3$ can be determined by applying certain boundary conditions (14)-(15).

M. Adel et al. / Eur. J. Pure Appl. Math, **18** (1) (2025), 5700

11 of 19

4. Verification of Adomian Decomposition Approach

Through a comparison with the results from the body of previous research, particularly the work by Sajid et al. [16]. Table 1 confirms for the current findings. Validating the results acquired by the Mohand transform and the Adomian decomposition approach is the goal of this comparison. The Prandtl number Pr represents the numerical values of the following comparison with $R = Z_b = M = Z_t = 0$. The precision and dependability of the results of the current investigation are demonstrated by this comparison. It is evident from the comparison that the existing research approach and its outcomes are credible.

Table 1. $-\theta'(0)$ values in varying Pr with $R = Z_b = M = Z_t = 0$

Pr	Sajid et al. [16]	Present work
1.0	0.556065	0.556064892
1.5	0.727928	0.727927745
2.0	0.873992	0.873991029
2.5	1.012056	1.012055496

5. Results and Discussion

This section aims to demonstrate the influence of temperature, concentration, velocity, the local Sherwood number, the skin friction coefficient, and the local Nusselt number as affected by the following parameters: chemical reaction parameter, Brownian motion parameter, magnetic parameter, thermophoresis parameter, Bingham number, Reiner-Philippoff fluid constraint, solutal relaxation time parameter, activation energy parameter, Eckert number, Prandtl number, and temperature. The Adomian decomposition method, grounded in the Mohand transform, offers a numerical characterization of the system governing the model under certain physical conditions. A variation in the magnetic parameter M can influence the flow behavior, as illustrated in Figure 2, which demonstrates the impact of the magnetic field parameter on temperature $\theta(\eta)$, concentration $\phi(\eta)$, and velocity $f'(\eta)$. Graphing the data indicates that increasing the magnetic parameter M reduces the velocity gradient, enhances the temperature of the nanofluid, and slightly increases concentration. The fluid's velocity diminishes due to elevated magnetic parameter values generating a Lorentz force that counteracts fluid motion.
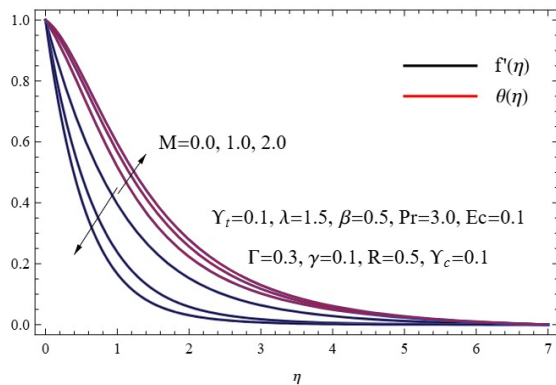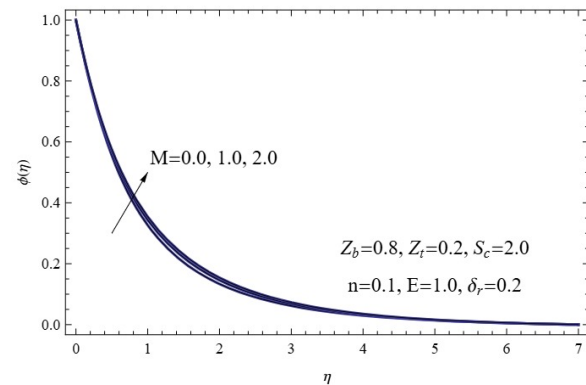
Figure 2 (a) $\theta(\eta)$ and $f'(\eta)$ for assorted M (b) $\phi(\eta)$ for assorted M

Reiner-Philippoff nanofluid flow behavior in terms of temperature $\theta(\eta)$, concentration $\phi(\eta)$, and velocity $f'(\eta)$ is illustrated in Figure 3 as a function of the Bingham number γ. First, it's crucial to understand that a Newtonian fluid is indicated by a Bingham number of zero ($\gamma = 0$). Stated differently, a fluid that exhibits $\gamma = 0$ shows no yield stress and, as a result, follows the standard Newtonian fluid behavior in which the viscosity is independent of the applied shear rate. The graph demonstrates that while the fluid's concentration and velocity climb with increasing Bingham number, the thermal gradient falls. This happens because a fluid is more resistant to deformation when its Bingham number is larger, which denotes a bigger yield stress. Because of the increased internal friction, this increased resistance decreases heat transfer. In addition, by promoting more consistent flow and improved particle distribution, the increased yield stress allows for higher fluid velocities and concentrations.
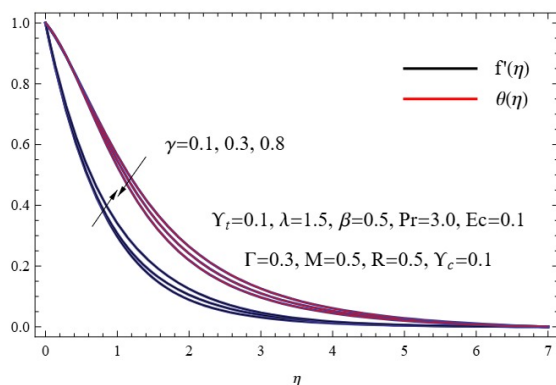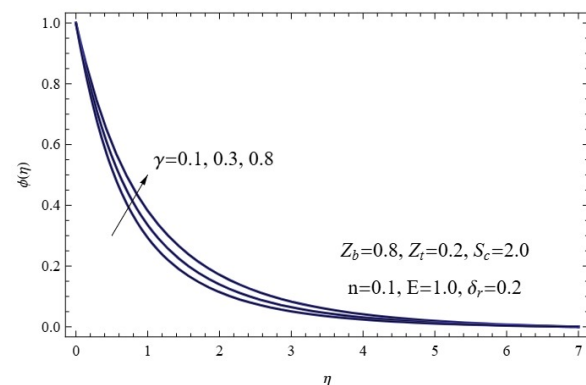

Figure 3 (a) $\theta(\eta)$ and $f'(\eta)$ for assorted γ (b) $\phi(\eta)$ for assorted γ

The Reiner-Philippoff parameter's λ behavior about the temperature $\theta(\eta)$, velocity $f'(\eta)$, and concentration $\phi(\eta)$ fields is depicted in Figure 4. Firstly, we must remember that the fluid also exhibits Newtonian behavior at $\lambda = 1$, with a constant viscosity that remains constant at different shear rates. On the other hand, when λ is less than 1, the fluid is considered dilatant, indicating that its viscosity increases as the shear rate increases,

making it more resistant to flow under larger stresses. In contrast, the fluid is considered pseudo-plastic when $\lambda > 1$, meaning that when the shear stress increases, it will flow more readily due to its decreasing viscosity with increasing shear rate. The graph indicates that the pseudo-plastic fluid's concentration and velocity exceed those of the dilatant and Newtonian fluids when the Reiner-Philippoff parameter improves. By contrast, an inverse correlation exists between the temperature fields and the Reiner-Philippoff parameter.
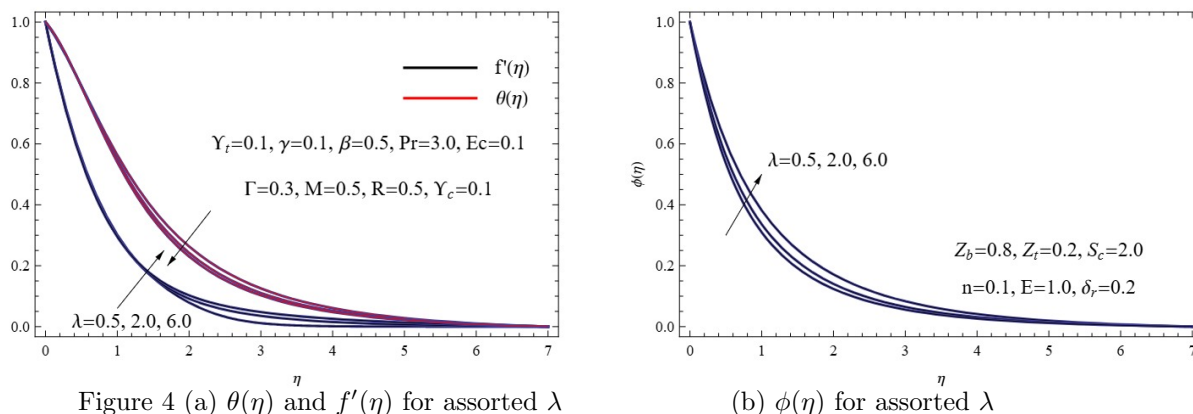

Figure 4 (a) $\theta(\eta)$ and $f'(\eta)$ for assorted λ (b) $\phi(\eta)$ for assorted λ

Figure 5 shows the impact of thermal relaxation time parameter Υ_t and solutal relaxation time parameter Υ_c on concentration and thermal fields. As the thermal relaxation time parameter increases, the thermal gradient increases and the concentration field decreases. A steeper temperature gradient is the result of heat diffusing over a longer period, which may be described physically by the longer thermal relaxation time. Yet, the concentration field decreases when heat is dispersed over a greater area because the thermal gradients that drive the concentration distribution are less strong. Moreover, the concentration gradient rises, and the associated thermal field falls with a boost in the solutal relaxation time parameter. This is physically accounted for by the fact that the thermal field drops as a result of the modified concentration dynamics, but the concentration gradient is enhanced by the longer solutal relaxation time, which allows the solute to accumulate more effectively.
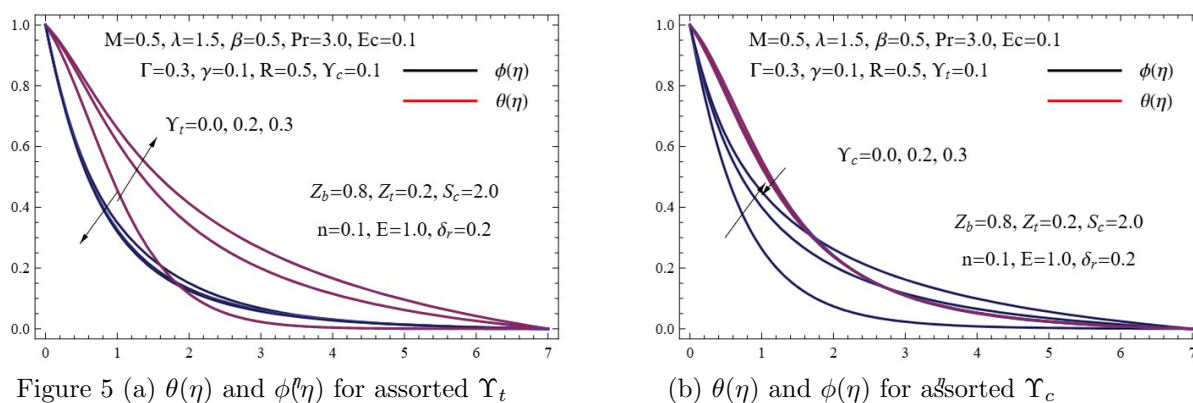

Figure 5 (a) $\theta(\eta)$ and $\phi(\eta)$ for assorted Υ_t (b) $\theta(\eta)$ and $\phi(\eta)$ for assorted Υ_c

Figure 6 shows the impact of gradients in temperature $\theta(\eta)$ and concentration $\phi(\eta)$ for increasing radiation parameter R and Eckert number Ec values. The graph shows that while concentration distribution falls, thermal distribution is enhanced by rising values of the radiation parameter or Eckert number. The reason for this is that higher radiation promotes heat transfer, which results in a more even distribution of heat, and higher Eckert numbers enhance viscous dissipation and heat creation. Since temperature-driven solute transport is reduced as a result of the higher thermal effects, the concentration gradient is lowered.
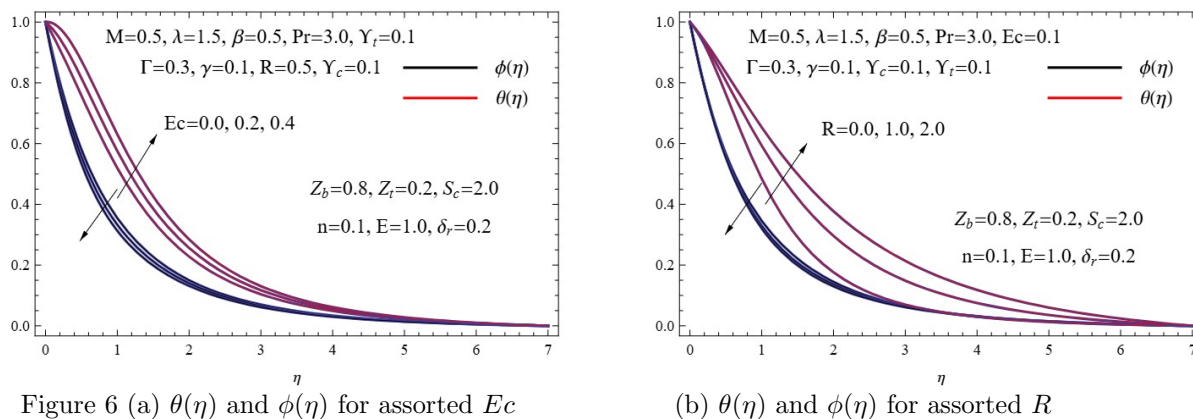

Figure 6 (a) $\theta(\eta)$ and $\phi(\eta)$ for assorted Ec (b) $\theta(\eta)$ and $\phi(\eta)$ for assorted R

Figure 7 depicts the influence of the Brownian motion parameter Z_b and the thermophoresis parameter Z_t on the thermal $\theta(\eta)$ and concentration $\phi(\eta)$ fields. The plotted figure demonstrates the increase in temperature distribution and the decrease in concentration distribution as the Brownian motion parameter escalates. Furthermore, an improvement in the temperature and concentration fields is brought about by the thermophoresis parameter's expanding values. The improvement in thermal and concentration distributions can be attributed to the enhanced thermophoresis, which propels particles from warmer to colder areas with greater efficiency.
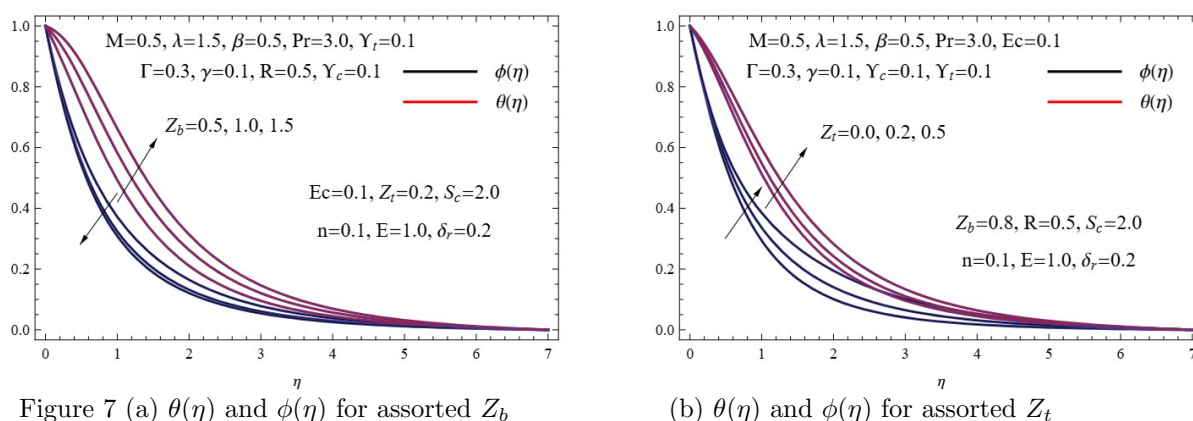

Figure 7 (a) $\theta(\eta)$ and $\phi(\eta)$ for assorted Z_b (b) $\theta(\eta)$ and $\phi(\eta)$ for assorted Z_t

Figure 8 displays the concentration profile change for various values of the chemical reaction parameter δ_r or the activation energy parameter E. In this case, the mass distribution is enhanced by greater activation energy parameter values while it is weakened by higher chemical reaction parameter values. This can be explained physically as faster chemical reaction rates use more reactants, which reduces mass distribution, but increases activation energy makes it simpler for particles to overcome energy barriers, enhancing mass distribution.
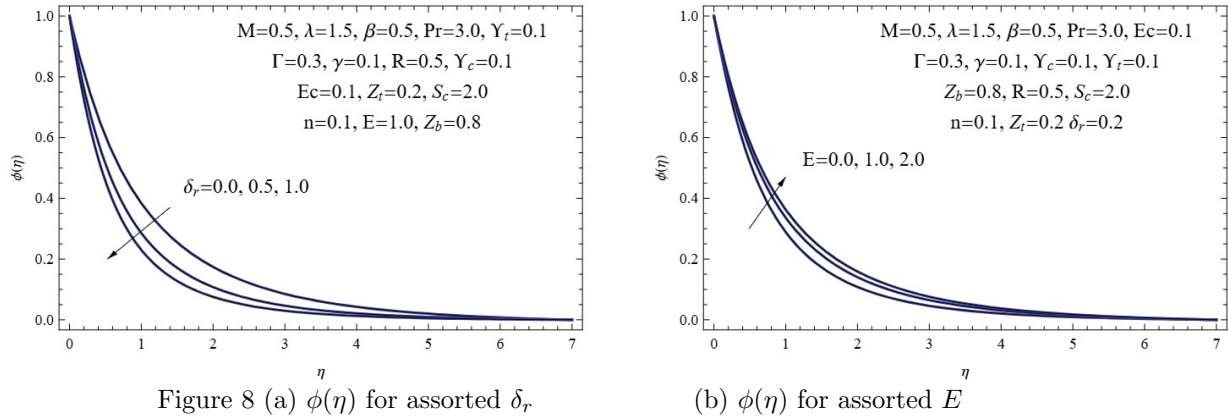

Figure 8 (a) $\phi(\eta)$ for assorted δ_r (b) $\phi(\eta)$ for assorted E

Skin friction $(Cf_x Re^{\frac{1}{2}})$, Sherwood number $(Sh_x Re^{\frac{-1}{2}})$, and Nusselt number $(Nu_x Re^{\frac{-1}{2}})$ fluctuations in response to various controlling parameters are shown in Table 2. These parameters affect the mass transfer rate, heat transfer rate, and surface friction, respectively. The data show how these modifications affect these parameters. In the domains of fluid dynamics, heat transfer, and mass transfer, in particular, these values are crucial. Systems in engineering applications like heat management, chemical processing, and aerospace require them to be carefully designed and optimized. Richer skin friction coefficient and poorer local Nusselt number are caused by rising amounts of the magnetic field parameter, Bingham number, and Reiner-Philippoff fluid.

Table 2. $Sh_x Re^{\frac{-1}{2}}$, $Cf_x Re^{\frac{1}{2}}$, and $Nu_x Re^{\frac{-1}{2}}$ as function of some of governing parameters with
$\beta = 0.5, Sc = 2.0, n = 0.1, Pr = 3.0, E = 1.0$ and $\Gamma = 0.3$

M	γ	λ	Υ_t	Υ_c	Ec	R	Z_b	Z_t	δ_r	$Cf_x Re^{\frac{1}{2}}$	$Nu_x Re^{\frac{-1}{2}}$	$Sh_x Re^{\frac{-1}{2}}$
0.0	0.1	1.5	0.1	0.1	0.1	0.5	0.8	0.2	0.2	0.881327	0.538817	1.18721
1.0	0.1	1.5	0.1	0.1	0.1	0.5	0.8	0.2	0.2	1.394642	0.358658	1.16321
2.0	0.1	1.5	0.1	0.1	0.1	0.5	0.8	0.2	0.2	1.750413	0.232276	1.15214
0.5	0.1	1.5	0.1	0.1	0.1	0.5	0.8	0.2	0.2	1.170692	0.464874	1.02306
0.5	0.3	1.5	0.1	0.1	0.1	0.5	0.8	0.2	0.2	1.200923	0.435463	1.17507
0.5	0.8	1.5	0.1	0.1	0.1	0.5	0.8	0.2	0.2	1.270380	0.405517	1.33093
0.5	0.1	0.5	0.1	0.1	0.1	0.5	0.8	0.2	0.2	1.150791	0.469372	1.02313
0.5	0.1	2.0	0.1	0.1	0.1	0.5	0.8	0.2	0.2	1.178753	0.436178	1.17256
0.5	0.1	6.0	0.1	0.1	0.1	0.5	0.8	0.2	0.2	1.226634	0.407493	1.27121
0.5	0.1	1.5	0.0	0.1	0.1	0.5	0.8	0.2	0.2	1.170692	0.514926	1.16189
0.5	0.1	1.5	0.2	0.1	0.1	0.5	0.8	0.2	0.2	1.170692	0.378464	1.18108
0.5	0.1	1.5	0.3	0.1	0.1	0.5	0.8	0.2	0.2	1.170692	0.340872	1.18647
0.5	0.1	1.5	0.1	0.0	0.1	0.5	0.8	0.2	0.2	1.170692	0.395878	1.26859
0.5	0.1	1.5	0.1	0.2	0.1	0.5	0.8	0.2	0.2	1.170692	0.479547	1.08722
0.5	0.1	1.5	0.1	0.3	0.1	0.5	0.8	0.2	0.2	1.170692	0.515606	1.01995
0.5	0.1	1.5	0.1	0.1	0.0	0.5	0.8	0.2	0.2	1.170692	0.609283	1.09733
0.5	0.1	1.5	0.1	0.1	0.2	0.5	0.8	0.2	0.2	1.170692	0.277313	1.19814
0.5	0.1	1.5	0.1	0.1	0.4	0.5	0.8	0.2	0.2	1.170692	0.047912	1.29726
0.5	0.1	1.5	0.1	0.1	0.1	0.0	0.8	0.2	0.2	1.170692	0.270952	0.27095
0.5	0.1	1.5	0.1	0.1	0.1	1.0	0.8	0.2	0.2	1.170692	0.579297	1.17214
0.5	0.1	1.5	0.1	0.1	0.1	2.0	0.8	0.2	0.2	1.170692	0.813973	1.13532
0.5	0.1	1.5	0.1	0.1	0.1	0.5	0.5	0.2	0.2	1.170692	0.665106	1.10042
0.5	0.1	1.5	0.1	0.1	0.1	0.5	1.0	0.2	0.2	1.170692	0.321876	1.19234
0.5	0.1	1.5	0.1	0.1	0.1	0.5	1.5	0.2	0.2	1.170692	0.127043	1.21107
0.5	0.1	1.5	0.1	0.1	0.1	0.5	0.8	0.0	0.2	1.170692	0.509556	1.19799
0.5	0.1	1.5	0.1	0.1	0.1	0.5	0.8	0.2	0.2	1.170692	0.437905	1.17259
0.5	0.1	1.5	0.1	0.1	0.1	0.5	0.8	0.5	0.2	1.170692	0.348344	1.16616
0.5	0.1	1.5	0.1	0.1	0.1	0.5	0.8	0.2	0.0	1.170692	0.467644	1.02194
0.5	0.1	1.5	0.1	0.1	0.1	0.5	0.8	0.2	0.5	1.170692	0.408185	1.35451
0.5	0.1	1.5	0.1	0.1	0.1	0.5	0.8	0.2	1.0	1.170692	0.377344	1.59455

Also, it is demonstrated that mass transfer is reduced by the solutal relaxation time parameter and enhanced by the chemical reaction parameter. This demonstrates their opposing effects on the mass transfer process, showing that a greater chemical reaction parameter speeds mass transfer while an increase in solutal relaxation time slows it down. Additionally, the same table shows that a rise in the Eckert number increases mass transmission while decreasing heat transfer. This is because greater viscous dissipation increases

species mixing, which enhances mass transfer, but also increases the amount of heat absorbed by the fluid, decreasing heat transfer efficiency. A little increase in the mass transfer rate and a decrease in the heat transfer rate are also observed when the Brownian motion parameter is raised. Additionally, since enhanced thermophoresis generates higher particle movement due to temperature gradients, it disrupts the uniform distribution of heat and mass and reduces transfer efficiency. As a result, raising the thermophoresis parameter values often lowers both mass and heat transfer rates.

6. Conclusions

Under consideration are activation energy, thermal radiation, Ohmic heating, and viscous dissipation in the flow of a hydromagnetic non-Newtonian Reiner-Philippoff nanofluid. The theory of Cattaneo-Christov double diffusions is used in place of the traditional Fick's and Fourier's laws during the modeling procedure. By adding relaxation durations into the diffusion equations, this method takes into account the finite speed of thermal and mass diffusions, resulting in a more accurate description of the actual processes. Mohand transform combined with the Adomian decomposition approach yields the numerical solution for the converted flow governing the model. The numerical findings' generated flow fields are shown while being influenced by several factors. Tabular data and graphics are utilized to leverage the limits on temperature concentration and velocity. The concentration profiles are enhanced by a surge in the Bingham number, the Reiner-Philippoff fluid parameter, and the solutal relaxation time parameter. The velocity scale grows as the Bingham number rises, but it decreases when the magnetic field parameter increases. In contrast to the chemical reaction parameter, concentration distribution improves with increasing the activation energy parameter. Higher chemical reaction parameter values cause the concentration layer to get more compact, whilst higher activation energy parameter values cause it to expand. A greater estimate of the magnetic field parameter, the Bingham number, and the Reiner-Philippoff fluid enriches the skin friction coefficient and impoverishes the local Nusselt number. About the solutal relaxation time parameter, mass transfer is shown to be reduced, whilst the chemical reaction parameter exhibits enhancing behavior.

Acknowledgements:

References

[1] W. Abbas, A. M. Megahed, and E. Fares. The impact of a chemical reaction on the heat and mass transfer mechanisms in a dissipative and radiative nanofluid flow over a nonlinear stretching sheet. *Scientific Reports*, 14:7712, 2024.

[2] A. Ahmad, M. Qasim, and S. Ahmed. Flow of reiner-philippoff fluid over a stretching sheet with variable thickness. *J. Braz. Soc. Mech. Sci. Eng.*, 39:4469–4473, 2017.

[3] N. A. N. Ariffin, I. Waini, A. R. M. Kasim, M. H. A. Kamal, M. R. Ilias, and S. A. Kechil. Flow and heat transfer analysis on reiner-philippoff fluid flow over a stretching sheet in the presence of first and second-order velocity slip and temperature jump effect. *CFD Letters*, 15:88–102, 2023.

[4] K. Benos, E. G. Karvelas, and I. E. Sarris. Crucial effect of aggregations in cnt-water nanofluid magnetohydrodynamic natural convection. *Therm. Sci. Eng. Prog.*, 11:263–271, 2019.

[5] S. Choi. Enhancing thermal conductivity of fluids with nanoparticles. *Am. Soc. Mech. Eng. Fluids Eng.*, 231:99–105, 1995.

[6] B. M. Faraj, D. T. M. Salih, B. H. Z. H. Ali, B. M. Hussien, S. A. Mahmood, and S. A. Hama. On the numerical solution for a two-dimensional laplace equation with initial boundary conditions by using finite difference methods. *Journal of Studies in Science and Engineering*, 2:50–59, 2022.

[7] U. Farooq, H. Waqas, M. Imran, A. Albakri, and T. Muhammad. Numerical investigation for melting heat transport of nanofluids due to stretching surface with cattaneo-christov thermal model. *Alexandria Eng. J.*, 61:6635–6644, 2022.

[8] Hashim and M. Khan. On cattaneo-christov heat flux model for carreau fluid flow over a slendering sheet. *Results in Physics*, 7:310–319, 2017.

[9] T. Hayat, A. Aziz, T. Muhammad, and A. Alsaedi. Three-dimensional flow of prandtl fluid with cattaneo-christov double diffusion. *Results in Physics*, 9:290–296, 2018.

[10] V. J. Jalal, B. M. Faraj, D. T. M. Salih, S. S. Abdulkareem, B. H. Z. H. Ali, B. M. Hussien, S. A. Mahmood, and S. A. Hama. Numerical solution for time period of simple pendulum under magnetic field. *Journal of Studies in Science and Engineering*, 2:60–66, 2022.

[11] K. G. Kumar, M. G. Reddy, M. I. Khan, F. Alzahrani, M. I. Khan, and E. R. El-Zahar. Heat transfer and melting flow of a reiner-philippoff fluid over a surface with darcy-forchheimer medium. *Case Studies in Thermal Engineering*, 28:101649, 2021.

[12] K. G. Kumar, M. G. Reddy, M. V. V. N. L. Sudharani, S. A. Shehzad, and A. J. Chamkha. Cattaneo-christov heat diffusion phenomenon in reiner-philippoff fluid through a transverse magnetic field. *Phys. Stat. Mech. Its Appl.*, 541:123330, 2020.

[13] T. Y. Na. Boundary layer flow of reiner-philippoff fluids. *Int. J. Non-Linear Mech.*, 29:871–877, 1994.

[14] M. E. Nasr, M. G. Reddy, W. Abbas, A. M. Megahed, E. Awwad, and K. M. Khalil. Analysis of non-linear radiation and activation energy analysis on hydromagnetic reiner-philippoff fluid flow with cattaneo-christov double diffusions. *Mathematics*, 10:1534, 2022.

[15] A. C. V. Ramudu, K. A. Kumar, V. Sugunamma, and N. Sandeep. Heat and mass transfer in mhd casson nanofluid flow past a stretching sheet with thermophoresis and brownian motion. *Heat Transfer*, 49:5020–5037, 2020.

[16] T. Sajid, M. Sagheer, and S. Hussain. Impact of temperature-dependent heat source/sink and variable species diffusivity on radiative reiner-philippoff fluid. *Math.*

Probl. Eng., page 9701860, 2020.

[17] R. Shah, U. Farooq, H. Khan, D. Baleanu, P. Kumam, and M. Arif. Fractional view analysis of third-order kortewege-de vries equations, using a new analytical technique. *Frontiers in Physics*, 7:244, 2020.

[18] A. Sudhanshu, M. Rashmi, and K. Anuj. A comparative study of mohand and elzaki transforms. *Global Journal of Engineering Science and Researches*, 6:203–213, 2019.

[19] J. Sui, L. Zheng, and X. Zhang. Boundary layer heat and mass transfer with cattaneo-christov double-diffusion in upper-convected maxwell nanofluid past a stretching sheet with slip velocity. *Int. J. Thermal Sci.*, 104:461–468, 2016.

[20] A. Ullah, E. O. Alzahrani, Z. Shah, M. Ayaz, and S. Islam. Nanofluids thin film flow of reiner-philippoff fluid over an unstable stretching surface with brownian motion and thermophoresis effects. *Coatings*, 9:21–32, 2018.

[21] N. J. Vidyarani, K. G. Kumar, R. Padmavathi, H. J. Mahesh, Lokesh, D. G. Prakasha, and V. S. S. Kumar. Magnetic swirling flow and cattaneo-christov heat and mass flux over a stretchable cylinder: A dual stratification model. *Ain Shams Engineering Journal*, 15:102869, 2024.

[22] N. J. Vidyarani, M. M. Mahesh, Praveena, D. G. Prakasha, M. R. Krishanamurthy, K. G. Kumar, D. Abduvalieva, and M. I. Khan. A comparative study of flow and c-c heat flux over a magnetic field under the influence of nanomaterial and carbon nanotubes. *Partial Differential Equations in Applied Mathematics*, 10:100696, 2024.